

**Key Points:**

- A pseudo-Lagrangian transformation was applied to diagnose the shape of a phytoplankton patch
- The pseudo-Lagrangian transformation allowed estimation of Chl-a fluorescence net rates of change
- Net biological production was comparable with in vitro estimates from dilution experiments under similar hydrographic conditions

Supporting Information:

Supporting Information may be found in the online version of this article.

Correspondence to:

B. Mourino-Carballido,
bmourino@uvigo.es

Citation:

Villamaña, M., Franks, P. J. S., Fernández Castro, B., Gilcoto, M., Marañón, E., & Mourino-Carballido, B. (2021). A pseudo-Lagrangian transformation to study a chlorophyll-a patch in the Ría de Vigo (NW Iberian Peninsula). *Journal of Geophysical Research: Oceans*, 126, e2021JC017455. <https://doi.org/10.1029/2021JC017455>

Received 26 APR 2021

Accepted 5 OCT 2021

A Pseudo-Lagrangian Transformation to Study a Chlorophyll-a Patch in the Ría de Vigo (NW Iberian Peninsula)

M. Villamaña¹, P. J. S. Franks² , B. Fernández Castro³ , M. Gilcoto⁴ , E. Marañón¹ , and B. Mourino-Carballido¹

¹Centro de Investigación Mariña, Universidade de Vigo, GOB, Vigo, Spain, ²Scripps Institution of Oceanography, University of California, San Diego, La Jolla, CA, USA, ³Ocean and Earth Science, University of Southampton, National Oceanography Centre, Southampton, UK, ⁴Instituto de Investigación Mariñas, Consejo Superior de Investigaciones Científicas, Vigo (Pontevedra), Spain

Abstract Because of the difficulties in tracking a water mass over time and conducting synoptic surveys over large spatial scales, measurements of biological variables in the ocean are often restricted to isolated Eulerian observations. Here a proof-of-concept of a pseudo-Lagrangian transformation was applied to a time series of chlorophyll-a profiles acquired at a single fixed station to diagnose the shape of a phytoplankton patch, and its physical-biological rates of transformation. During August 2013, a 27-hr time series of observations of horizontal currents, hydrographic properties, turbulent mixing and chlorophyll-a was acquired at a central station of the Ría de Vigo (NW Iberian Peninsula). A chlorophyll-a patch, tilted upward toward the inner part of the Ría, was observed moving back and forth past the sampling station. Its shape and position during the sampling period were modulated by the semi-diurnal (M2) tidal currents and the vertically sheared upwelling circulation. The pseudo-Lagrangian transformation allowed estimation of chlorophyll-a net rates of change. These rates were positive between 12 and 14 m depth, and negative elsewhere, with a mean value of $-0.001 \pm 0.449 \text{ days}^{-1}$ within the patch maximum. After accounting for the effects of diffusion and sinking, the mean net biological production rate in the upper 15 m ($0.53 \pm 0.25 \text{ days}^{-1}$) was comparable with in vitro estimates of the balance between phytoplankton growth and mortality obtained from dilution experiments carried out under similar conditions ($0.2 \pm 0.7 \text{ days}^{-1}$). This pseudo-Lagrangian transformation is complementary to traditional analyses for the quantification of ecological processes and biogeochemical budgets.

Plain Language Summary Oceanography distinguishes two ways to make observations: Eulerian and Lagrangian. Eulerian approaches measure properties at fixed locations in space as a function of time as water flows past the instrument. In contrast, Lagrangian approaches quantify temporal changes in fluid parcels while following the flow. Isolated Eulerian observations are the most common approach to investigate biological properties. However, temporal variations in Eulerian observations result from combinations of physical and biological processes whose effects are often difficult to separate. We applied a pseudo-Lagrangian methodology to reconstruct the spatial structure of a phytoplankton (microscopic algae) patch observed at a single station in a coastal embayment. Because the flow was dominated by tidal currents, some water parcels were sampled multiple times, allowing to compute the rate of change of properties in the phytoplankton patch. Biological production, or the rate of change due to biological processes, was comparable with traditional estimates from in vitro experiments performed in the region under similar hydrographic conditions. Our findings show that the pseudo-Lagrangian transformation is a useful complement to data obtained from traditional analyses for the quantification of ecological processes and biogeochemical budgets.

1. Introduction

Coastal embayments and estuaries respond to a variety of forcing mechanisms over a wide range of timescales (Wong & Moses-Hall, 1998). Considering the wide range of temporal and spatial scales that determine the physical and biological coupling in these regions, multidisciplinary methodological approaches are required to determine the factors that control phytoplankton growth and composition. Traditionally,

oceanography, and fluid dynamics in general, distinguish two ways to make observations: Eulerian and Lagrangian. In the Eulerian approaches, properties are measured at fixed locations in space as a function of time as water flows past the instrument. In contrast, Lagrangian approaches quantify changes in fluid parcels while moving with them in space and time. Thus, for example, measurements from a free-floating drifter in the ocean are quasi-Lagrangian (floating instruments do not follow vertical flows), whereas measurements from a moored buoy are Eulerian. In general, biological variables and rates are difficult to measure in the ocean as the intense sampling required, both on the ship and subsequently in the lab, limits the spatial and temporal resolution with which they can be examined. These isolated Eulerian observations are then interpolated and extrapolated to infer dynamics over larger spatial and temporal scales. However, temporal variations in Eulerian observations at a single station result from combinations of physical and biological processes whose effects are often difficult to separate.

The Ría de Vigo is the southernmost of the Rías Baixas, four V-shaped coastal embayments located in the NW Iberian Peninsula that are part of the Iberia-Canary Current Upwelling System. The semi-diurnal (M2) tide and a residual estuarine circulation are the main driving forces affecting the Ría's circulation. Local and shelf wind affect the residual circulation of the Ría, driving coastal upwelling-downwelling events and causing vertically sheared exchange flows along the main channel (Gilcoto et al., 2001; Piedracoba et al., 2005). The upwelling brings cold and nutrient-rich Eastern North Atlantic Central Water (ENACW) (Ríos et al., 1992) as a lower layer into the Ría, whereas during downwelling oceanic warmer surface waters flow into the Ría (Barton et al., 2016). In general, upwelling-downwelling events follow a seasonal pattern: northerly winds predominate from April to September causing upwelling, whereas southerly winds from October to March favor downwelling. However, shifting wind patterns cause a succession of upwelling and downwelling episodes over shorter timescales (~3 days) (Álvarez-Salgado et al., 2000; Gilcoto et al., 2017). The nutrient-rich upwelled water stimulates phytoplankton primary production, which sustains an important fishing and shellfish industry such as mussel production (Blanton et al., 1987; Figueiras et al., 2002). Phytoplankton biomass presents a bimodal pattern with the maxima found during the seasonal transitions from downwelling to upwelling (spring) and from upwelling to downwelling (autumn) (Figueiras et al., 2002). Moreover, the phytoplankton community follows a seasonal succession in dominance patterns, with diatom dominance in spring, a progressive contribution of heterotrophic components during summer, and a major contribution of dinoflagellates in late summer and early autumn (Figueiras & Niell, 1987; Pitcher et al., 2010).

In this study, a proof-of-concept of a pseudo-Lagrangian technique was applied to transform chlorophyll-a fluorescence concentrations measured in the Ría de Vigo from an Eulerian to a pseudo-Lagrangian frame. The Eulerian to pseudo-Lagrangian transformation is commonly applied in atmospheric sciences to estimate tracer fields and rates (Bowman et al., 2013; Dragani et al., 2002; Nilsson & Leck, 2002) and in many ocean studies based on satellite data (d'Ovidio et al., 2004, 2010) or models (Doglioli et al., 2006). However, the use of this technique to study the evolution of in situ tracer data in the ocean has been limited by the lack of highly resolved physical data sets acquired simultaneously with biological measurements. To our knowledge, only a single study has applied the pseudo-Lagrangian transformation to chlorophyll-a as the tracer of interest (de Verneil & Franks, 2015). These authors applied this technique to re-map temporally sequential samples acquired on a spatial grid back to a presumed initial condition at a single time, based on the local flow. In doing so, the investigators generated a temporally synoptic chlorophyll-a fluorescence map in the California Current Ecosystem in summer 2012. This pseudo-Lagrangian re-mapping also showed which water parcels were sampled more than once, allowing estimation of chlorophyll-a net rates of change that could not have been obtained using traditional in vitro methods (e.g., in situ dilution methods or primary production measurements). In our study, the pseudo-Lagrangian methodology was applied to reconstruct the spatial structure of a chlorophyll-a fluorescence patch observed at a single station as the water moved past. This spatial reconstruction allowed us to identify water parcels that were sampled multiple times, and thus to compute net rates of change of chlorophyll-a fluorescence.

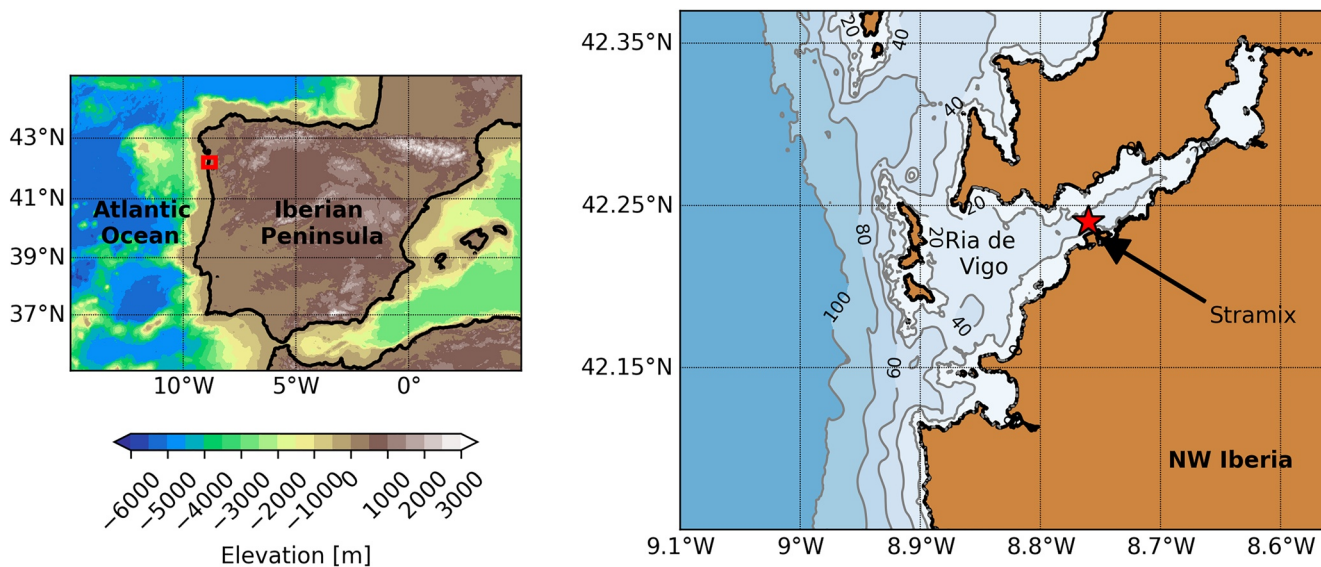


Figure 1. Map showing the position of the sampling station (STRAMIX, 42.24°N–8.76°W) where high-frequency observations were carried out in the Ría de Vigo on 5–6 August 2013.

2. Materials and Methods

The sampling station (42.24°N–8.76°W) was located in the central part of the Ría de Vigo (NW Iberian Peninsula) at the main channel (Figure 1). On 5–6 August 2013, an oceanographic cruise was conducted on board the R/V Mytilus over a period of 27 hr, during which we obtained high-frequency observations of hydrographic properties, microstructure turbulence, and horizontal currents.

2.1. Hydrographic and Microstructure Turbulence Data

An intensive sampling (yo-yo) of hydrography and microstructure turbulence data was accomplished by using a MSS90 profiler (Prandke & Stips, 1998), obtaining a total of 505 profiles with an averaged sampling interval of 3 min. The profiler was equipped with two microstructure shear sensors (type PNS06), a microstructure temperature sensor (FP07), a high-precision CTD (Conductivity Temperature Depth) probe including a fluorescence sensor, and a sensor to measure the horizontal acceleration of the profiler. The acquisition and processing of the data were performed with the commercial software SST-SDA (Standard Data Acquisition) and ProDat Sea & Sun Technology (<http://www.sea-sun-tech.com/technology.html>). Dissipation rates of turbulent kinetic energy (ε) were derived by integration of the wavenumber spectrum of the vertical shear as described in Fernández-Castro et al., (2014). The vertical diffusivity coefficient (K_z) was estimated as:

$$K_z = \Gamma \frac{\varepsilon}{N^2} \left(\text{m}^2 \text{s}^{-1} \right) \quad (1)$$

where N^2 is the buoyancy frequency squared and Γ is the mixing efficiency, which was assumed to take a constant value of 0.2, after the seminal work of Osborn (1980). Although we acknowledge that this parameter may not always be constant (it can depend on the sources of turbulence and the interplay between inertial and buoyancy forces, among other drivers), a consensus on an adequate parameterization for Γ is still lacking within the community, and the use of $\Gamma = 0.2$ remains a widely accepted choice until this consensus emerges (Gregg et al., 2018). This choice is particularly well justified for the Ría de Vigo, where the conditions are marginally unstable to shear-driven turbulence (Fernández-Castro et al., 2018) for which Γ approaches the canonical value (Smyth, 2020).

The fluorometer included in the MSS profiler was calibrated with fluorometrically determined surface chlorophyll a concentrations ranging from 0.03 to 8.60 mg m⁻³ [Chl a = 2.255 fluorescence – 0.527; $R^2 = 0.859$, number of samples (ns) = 134], obtained during 12 cruises carried out in three contrasting

marine environments. Three cruises (CARPOS October–November 2006, TRYNITROP April–May 2008 and MALASPINA December 2010–July 2011) sampled 72 stations, mainly located in the tropical and subtropical Atlantic and Pacific Oceans. Three cruises carried out in the Northwestern Mediterranean Sea (FAMOSO1 March 2009, FAMOSO2 April–May 2009, FAMOSO3 September 2009) sampled 16 stations during three contrasting hydrographic conditions, covering from winter mixing to summer stratification. In the Galician coastal upwelling 46 stations were sampled during six cruises, spanning all seasons and representative conditions: HERCULES1 HERCULES2 September 2011, HERCULES3 July 2012, DISTRAL February 2012–November 2012, CHAOS August 2013, and NICANOR February 2014–December 2015 cruises. More details are provided in Mouriño-Carballedo et al. (2021).

2.2. Current Data

A bottom-mounted upward-looking ADCP (Acoustic Doppler Current Profiler) was deployed at the sampling station from June 20, 2013 to August 13, 2014. The ADCP, a Teledyne RD Instruments WorkHorse 600 kHz, was configured to obtain current measurements at 60 levels (bins) of 0.75 m vertical extent at a sampling rate of 2 Hz that were averaged every minute. It was deployed at the 45 m isobath on a ballasted pyramid with a gimbal system to level it. Zonal and meridional velocity vector components were projected onto an axis along (u) and across (v) the main channel of the Ría (20° above East). The u and v components were positive to the Northeast (into the Ría) and to the Northwest, respectively. Sub-tidal residual (u^R) currents related to upwelling circulation were calculated by filtering out tidal frequencies (semi-diurnal and higher) with an A24/25/25 filter (Godin, 1972). The tidal and super-tidal currents, dominated by the semi-diurnal tide M2, were calculated as: $u^{M2} = u - u^R$.

2.3. Data Transformation to a Common Density and Time Framework

Chlorophyll-a fluorescence (MSS profiler) and horizontal current (ADCP) data were interpolated onto a common grid with a resolution of 1 m in the vertical dimension and 10 min in time from August 5, 2013 07:10:00 (Coordinated Universal Time, UTC) to August 6, 2013 10:10:00 (UTC). Because most flows occur along isopycnals, and in order to avoid vertical displacements of the chlorophyll-a patch due to the activity of internal waves, variables were displayed in potential density (σ_0 ; kg m⁻³) rather than pressure (depth) vertical coordinates.

2.4. Pseudo-Lagrangian Approach

The pseudo-Lagrangian approach consisted of converting the Eulerian time-depth (or in this case time-density) chlorophyll-a distribution measured at the station, into a pseudo-Lagrangian (flow-following) frame by use of the local Eulerian current velocities. It is assumed that each density surface moves as an independent slab, carrying its properties with it. This slab moves back and forth past the sampling station through tidal motions as samples are acquired. The pseudo-Lagrangian method uses the local velocity data to remap samples acquired in time, to infer what the sample distribution in space would have been, given the time-dependent velocity of a given layer.

First, chlorophyll-a profiles were back-adveected to the spatial location where they would have been at the start of the sampling ($t = 0$), or any arbitrary time during sampling. Knowing the time elapsed between the start of sampling and each observed chlorophyll-a profile, distances from the sampling point at each density slab were calculated using the local Eulerian velocity measurements $u(t,z)$:

$$x(t + \Delta t, z) = x(t, z) + u(t, z) \cdot \Delta t \quad (2)$$

where $x(t, z)$ is the distance in the along-Ría axis at a given time and depth, $u(t, z)$ is the along-Ría component of velocity at a given time and depth, t is the time, and Δt is the time between each profile ($\Delta t = 10$ min). Because across-Ría currents were small, the technique was only applied in the along-Ría axis. This equation allows us to predict the previous or subsequent spatial location of a sample acquired at the station at a given time and depth. Using this information, we can then use temporal changes in the distribution at a single location to infer the spatial distribution of the chlorophyll-a observations at a single time.

With an oscillatory current such as one driven by the tide, this pseudo-Lagrangian transformation produces a spatial reconstruction of the location of points sampled in time. In this spatial reconstruction, chlorophyll-a values were averaged into $0.2 \text{ km} \times 0.01 \text{ kg m}^{-3}$ along-Ría bins to obtain an average chlorophyll-a patch structure. This patch corresponds to the chlorophyll-a spatial distribution as it would have appeared if sampled instantaneously in space at the start of the sampling. The pseudo-Lagrangian reconstruction revealed that many water parcels were sampled multiple (three to four) times as the tide brought the waters back and forth past the station. The temporal evolution of chlorophyll-a in such water parcels allowed the calculation of the net rates of change of chlorophyll-a in the patch. Finally, using the average chlorophyll-a spatial distribution and the measured currents, a predicted chlorophyll-a time series was reconstructed by reversing the pseudo-Lagrangian transformation. This time series revealed what would have been sampled if the chlorophyll-a patch had not changed in time as it advected past the sampling station and could be compared to the original chlorophyll-a time series to diagnose changes in time and space.

2.5. Calculation of Net Rates of Change of Chlorophyll-a

A general equation to describe the time evolution of concentration (C) of a biogeochemical property at a fixed location is:

$$\frac{\partial C}{\partial t} + u \cdot \nabla C = \text{Diffusion} + \text{Swimming} + \text{Sources} - \text{Sinks} \quad (3)$$

Transforming to a Lagrangian frame eliminates horizontal advection ($u \cdot \nabla C$), as water velocities relative to the observation point are zero:

$$\frac{\partial C}{\partial t} = \text{Diffusion} + \text{Swimming} + \text{Sources} - \text{Sinks} \quad (4)$$

Chlorophyll-a is a proxy of phytoplankton biomass and its concentration in the ocean is controlled by biological and physical processes that affect phytoplankton cells. Phytoplankton growth rates depend on temperature, nutrients, and light availability, while biological loss rates include processes such as grazing, viral lysis, and natural mortality. In addition, phytoplankton is affected by physical diffusion, sinking, and active swimming. Therefore, after removing advection and neglecting other horizontal processes, the time evolution of chlorophyll-a (Chl-a) can be expressed as:

$$\frac{\partial Chl - a}{\partial t} = J_B - \frac{\partial F_{diff}}{\partial z} - \frac{\partial F_{sink}}{\partial z} - \frac{\partial F_{swim}}{\partial z} \left(\text{mg m}^{-3} \text{day}^{-1} \right) \quad (5)$$

where J_B is the net biological production term (biological production minus losses) and F_{diff} , F_{sink} , and F_{swim} are the vertical diffusive, sinking, and active swimming fluxes of chlorophyll-a, respectively.

The vertical diffusive flux of chlorophyll-a was estimated from the observations of vertical turbulent diffusivity as:

$$F_{diff} = -K_z \cdot \frac{\partial Chl - a}{\partial z} \left(\text{mg m}^{-2} \text{day}^{-1} \right) \quad (6)$$

where K_z is the time-mean vertical diffusivity profile and $\partial Chl - a / \partial z$ the time-mean vertical gradient of chlorophyll-a profiles calculated during the 27-hr sampling.

Sinking flux of chlorophyll-a was calculated as:

$$F_{sink} = -w \cdot Chl - a \left(\text{mg m}^{-2} \text{day}^{-1} \right) \quad (7)$$

where w is the cell sinking velocity and Chl-a is the averaged chlorophyll-a profile during the 27-h sampling. We took $w = 1-10 \text{ m day}^{-1}$ which, according to Miklasz and Denny (2010), corresponds to diatom cells in the range size 10–50 μm , typically dominant in the Ría de Vigo during summer (Cermeño et al., 2006; Figueiras & Pazos, 1991). Although data on phytoplankton composition were not available, previous studies in this ecosystem have shown that diatoms tend to dominate heavily the community during the upwelling-favorable season (Figueiras et al., 2002; Pitcher et al., 2010). We therefore assumed that motile species were not abundant and thus took the swimming term to be zero.

To calculate local net rates of change of chlorophyll-a ($\partial Chl - a / \partial t$) samples of the same water at different times are required. If the regions sampled twice have significantly different concentrations, then there must

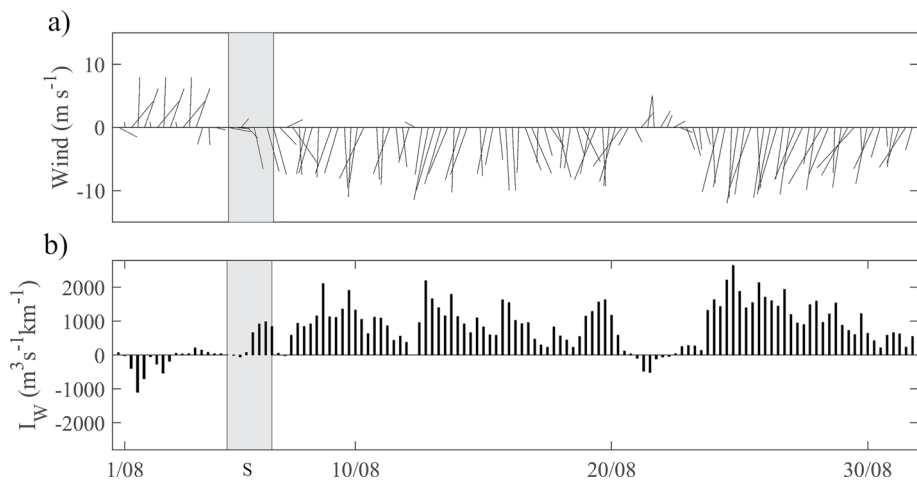


Figure 2. (a) Vector diagram of wind direction and speed (m s^{-1}) recorded at the Cabo Silleiro meteorological station (42.13°N 9.44°W). (b) Upwelling index (IW) calculated for the same period. Negative (positive) values correspond to northerly (southerly) wind and upwelling (downwelling), respectively. The shaded areas correspond to the sampling hours (S).

be a temporal evolution of the tracer in these water parcels. Only the $0.2 \text{ km} \times 0.01 \text{ kg m}^{-3}$ bins that were sampled at least twice with a $\Delta t > 6 \text{ hr}$ were selected. Finally, the biomass-normalized net rate of change for each bin was estimated by dividing the slope of the linear regression of chlorophyll-a and time, by the initial chlorophyll-a concentration. The rate of change due to diffusion and sinking was normalized by the mean chlorophyll-a concentration for the 27 hr sampling.

The errors in the different budget terms were estimated by repeating the calculation with randomly perturbed input profiles of K_z and chlorophyll-a, and values of the sinking velocity, w , following a Monte Carlo approach. Normally distributed perturbed values of K_z and chlorophyll-a at each depth were randomly generated using the mean and standard error of the corresponding variable at each depth. Perturbed values of w were generated by assuming boxcar distribution with values comprised between 1 and 10 m days^{-1} , following the description above.

3. Results

3.1. Hydrographic Conditions

Northerly winds and upwelling prevailed during August 2013, but the region was characterized by relaxation-downwelling conditions during most of July (Figure 5 in Villamaña et al., 2017) and early August (Figure 2). The sampling coincided with a transition from downwelling-relaxation to upwelling at the beginning, and an intensification of the upwelling at the end of the sampling period. This was reflected in the hydrographic properties of the water column (Figures 3 and 4). Current velocities were higher in the along-Ría than in the across-Ría axis (Figure 3). Maximum inflow (27 cm s^{-1}) and outflow (-25 cm s^{-1}) were higher in this direction compared to the across-Ría axis (8 and -13 cm s^{-1} , respectively). Currents exhibited a semi-diurnal tidal cycle in both axes, showing a tidal range close to spring tides (Fernández-Castro et al., 2018) and presenting larger velocities than the residual term. Furthermore, the residual currents in the along-Ría axis (u^R) exhibited a two-layer circulation, with outflow ($\sim 3 \text{ cm s}^{-1}$) above 10 m and inflow ($\sim 2 \text{ cm s}^{-1}$) below (10 – 35 m), which intensified ($\sim 5 \text{ cm s}^{-1}$) at the end of the sampling (from 18:00 onwards).

To assess the robustness of the one-dimensional pseudo-Lagrangian transformation, for which we assume that the across-Ría currents are comparably weak, we plotted the progressive velocity vectors at three representative (shallow, intermediate, and deep) density layers, for the total currents and the tidal currents alone (Figure 4). The progressive vectors of the total currents (upper panel) for the shallowest and deepest density levels align very closely with the bathymetry, but the middle one drifts weakly southward (indicating potentially a northerly origin of the water mass). This is likely related to the fact that this isopycnal is

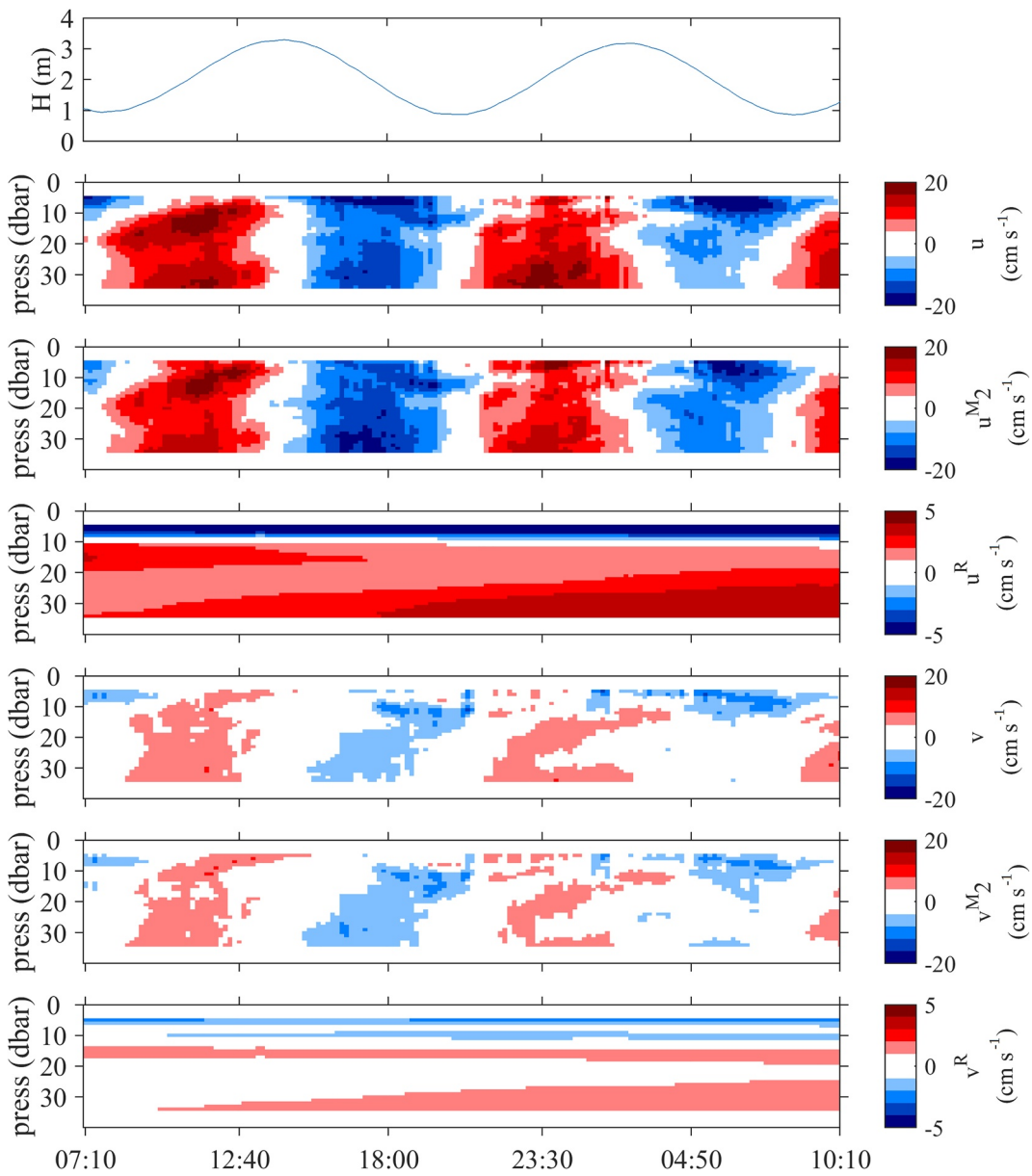


Figure 3. Acoustic Doppler Current Profiler (ADCP) currents along (u) and across (v) the Ría axis during the sampling period (5–6 August 2013). Residual currents calculated with a low-pass Godin 24/24/25 filter (u^R , v^R) and the corresponding high-passed currents dominated by the semi-diurnal tidal signal (u^{M2} , v^{M2}) are also represented. Tidal height is represented at the top. Horizontal scale corresponds to Coordinated Universal Time (UTC); local time was UTC+2.

located right at the node of the along-Ría velocity component, such that the across-Ría becomes important. The lower panel shows the tidal component and indicates that the tidal ellipses are highly elliptical and are even almost linear, showing barely no flow in the cross direction. These results support our simplification of considering exclusively the along-Ría component.

The water column showed thermal and haline stratification (Figure 5). Temperatures $>21^\circ\text{C}$ were observed at the surface and colder temperatures ($<14^\circ\text{C}$) in deeper waters, whereas salinity values ranged from 35.8 PSU (>15 m) to 35.1 PSU (surface). As the result of the observed thermal and haline stratification, higher values of buoyancy frequency squared (N^2) were observed in the upper 20 m ($1.4 \pm 1.0 \times 10^{-3} \text{ s}^{-2}$). In general, higher values of dissipation rates of turbulent kinetic energy (ε) were observed in the upper layers

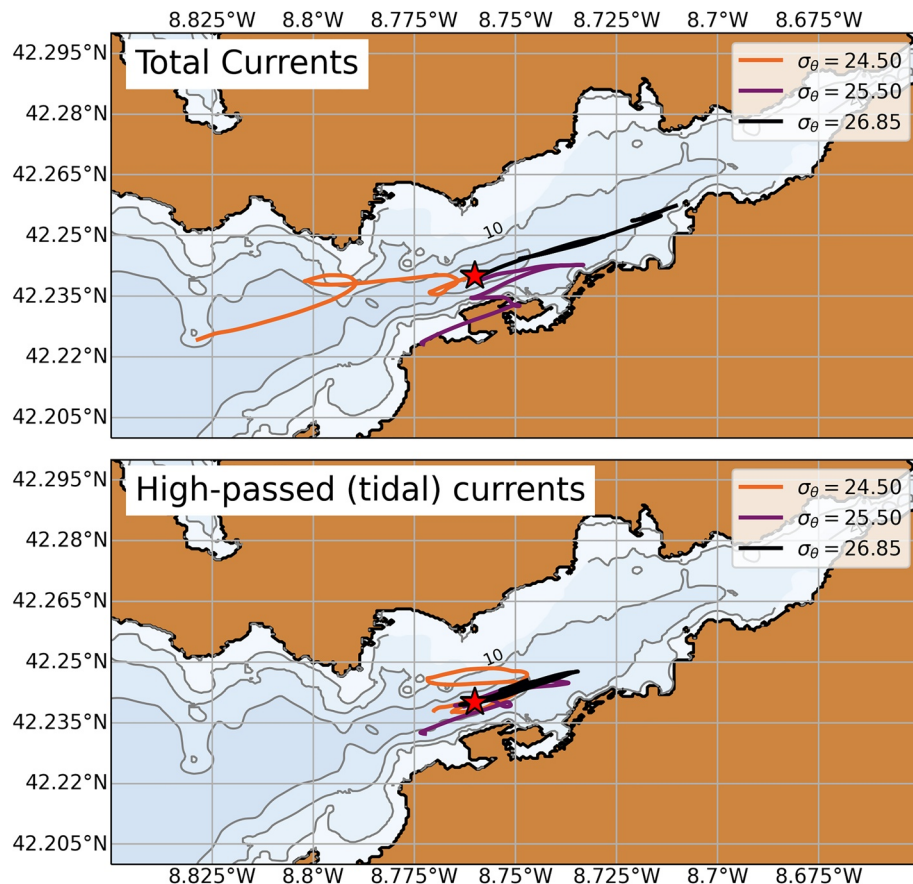


Figure 4. Progressive vector diagrams for the total currents (top) and high-passed tidal currents (bottom), for a shallow, intermediate, and deep density level.

($0.6 \pm 3.4 \times 10^{-6} \text{ m}^2 \text{ s}^{-3}$; 5–20 m), extending down to 10–20 m mainly during the night (from 20:30 to 06:00 h approximately). Vertical diffusivity (K_z), which is a function of the distributions of ε and N^2 (see Methods), was usually higher ($0.4 \pm 1.1 \times 10^{-4} \text{ m}^2 \text{ s}^{-1}$) close to the bottom (20–30 m). Higher values were also observed in the upper 20 m during the night ($0.3 \pm 6.4 \times 10^{-2} \text{ m}^2 \text{ s}^{-1}$), coinciding with the increase in ε and the upwelling intensification. The chlorophyll-a vertical distribution exhibited a subsurface maximum ($\sim 6 \text{ mg m}^{-3}$) at around 15 m, which diminished in intensity ($\sim 4 \text{ mg m}^{-3}$) during the night. When plotting chlorophyll-a versus density (Figure 6), it is clear that the chlorophyll-a maximum values extended between 25.5 and 26.5 kg m^{-3} density surfaces at low tides, whereas they were confined around 26.5 kg m^{-3} at high tides.

3.2. Pseudo-Lagrangian Reconstruction of the Chlorophyll-a Patch

The reconstructed shape of the chlorophyll-a patch at the beginning of the cruise (August 5, 2013 07:10) was obtained by using the Eulerian velocities to re-map the spatial positions of the chlorophyll-a observations at each measured time and density (Equation 3) to their inferred locations at the start of sampling ($t = 0$). The values corresponding to each $0.2 \text{ km} \times 0.01 \text{ kg m}^{-3}$ bin were then averaged to obtain an average two-dimensional chlorophyll-a distribution versus density and along-Ría distance (Figure 7). The number of observations per bin was higher around the sampling station, and from 25 to 25.5 kg m^{-3} in the density axis and also in the outer part of the patch from 26 to 26.5 kg m^{-3} (Figure 7a). The chlorophyll-a patch at the beginning of the observation was found to be tilted across isopycnals in the along-Ría axis, extending ~ 6 km from the sampling station toward the inner part ($x > 0$) of the Ría above 25.5 kg m^{-3} , and ~ 3 km toward the outer part ($x < 0$) of the Ría below 25.5 kg m^{-3} . The maximum chlorophyll-a values ($\sim 5\text{--}6 \text{ mg m}^{-3}$, red

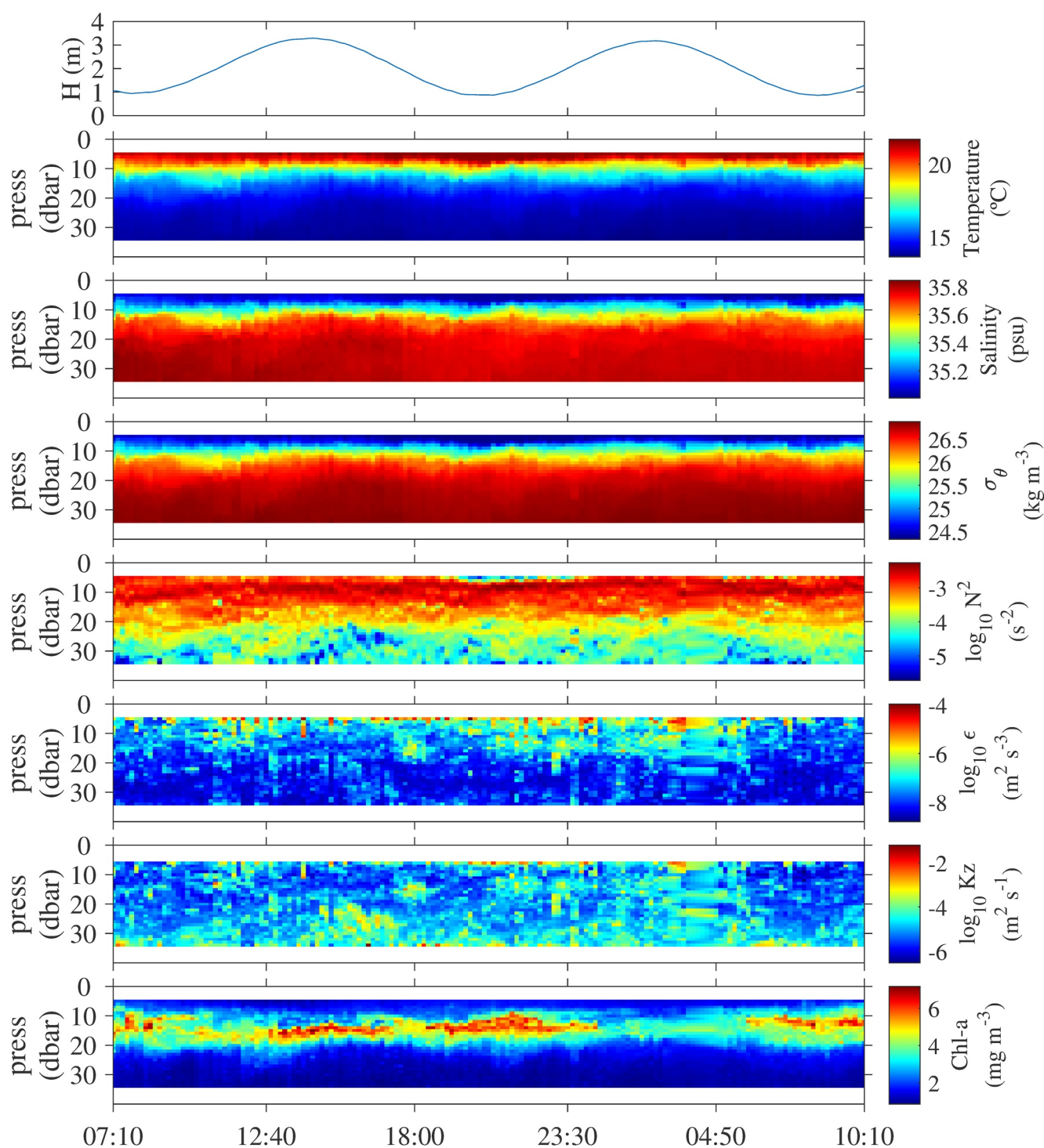


Figure 5. Vertical distribution of temperature, salinity, potential density (σ_{θ}), decimal logarithm of buoyancy frequency squared (N^2), decimal logarithm of dissipation rate of turbulent kinetic energy (ϵ), decimal logarithm of vertical diffusivity (K_z), and chlorophyll-a fluorescence derived from the microstructure profiler during the sampling period (5–6 August 2013). Tidal height is represented at the top. Horizontal scale corresponds to Coordinated Universal Time (UTC); local time was UTC+2.

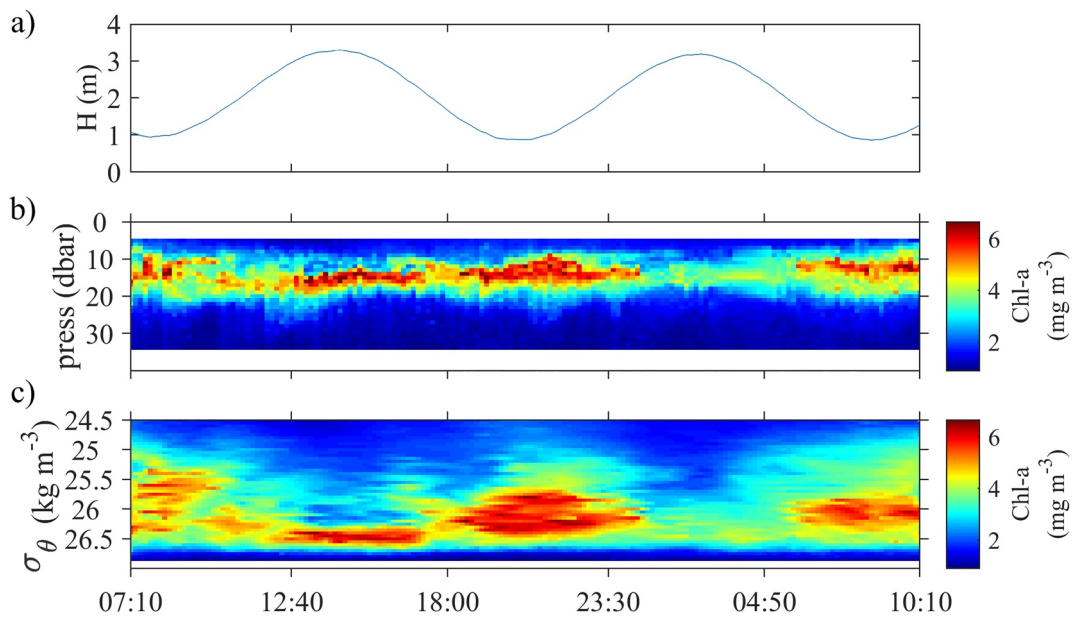


Figure 6. (a) Tidal height. (b) Eulerian distribution of chlorophyll-a in a vertical axis of pressure. (c) Eulerian distribution of chlorophyll-a in a vertical axis of potential density. Horizontal scale corresponds to Coordinated Universal Time (UTC); local time was UTC+2.

color) were found in a tilted layer between 25.5 and 26.5 kg m^{-3} in density and located toward the outer part of the Ría ($x < 0$).

After applying current velocities to the different density surfaces to construct the initial shape of the chlorophyll-a patch (Figure 7), we could then use this patch structure and the currents to reconstruct changes in the spatial structure of the patch at different times. Figure 8 shows five snapshots of the chlorophyll-a patch (panels a–e) corresponding to different times during the original Eulerian observations (dotted lines a–e), enabling us to see which parts of the chlorophyll-a patch were sampled at each time. At times A, C, and E, coinciding approximately with low tides, the wide zone of the chlorophyll-a patch located toward the inner part ($x > 0$) of the Ría was sampled (solid vertical line), whereas at high tides, we sampled the narrow area located toward the external part ($x < 0$) of the Ría (times B, D). From 20:30 h approximately, the chlorophyll-a patch started to un-tilt due to the vertical shear of the mean flow, until it became almost vertical at time E (Figure 8c). This reversal coincided with intensification of the upwelling and an increase in vertical mixing observed at the surface and intermediate depths (Figure 5). See also Movie S1 for a description of the temporal evolution of the shape of the chlorophyll-a patch. Finally, a predicted chlorophyll-a time series was reconstructed by reversing the pseudo-Lagrangian transformation (Figure 9). In general, the reconstructed chlorophyll-a time series was very similar to the original Eulerian observation. White areas indicate those regions of the patch where we did not get enough coverage to reconstruct it.

3.3. Net Rates of Change of Chlorophyll-a

The temporal evolution of chlorophyll-a fluorescence values obtained at re-sampled water parcels were used to compute net rates of change. The biomass-normalized net rate of chlorophyll-a change ($\partial Chl - a / \partial t$) was calculated only in the $0.2 \text{ km} \times 0.01 \text{ kg m}^{-3}$ bins (Figure 10) that were sampled at least twice within a time interval $\Delta t > 6 \text{ h}$. A total of 152 estimates of chlorophyll-a net rate of change were obtained within the patch; these ranged from -1.05 to 1.08 days^{-1} , with zones that consistently showed net increase (>0) and zones that showed net loss (<0). The averaged chlorophyll-a net rate of change for the patch during the sampling period and the chlorophyll-a diffusion and sinking fluxes and rates based on the mean chlorophyll-a profile are shown in Figure 11 in depth vertical coordinates. The difference of the chlorophyll-a net rate of change with diffusion and sinking rates constitutes the biological net production (J_B). The chlorophyll-a net rate of change ($\partial Chl - a / \partial t$) was positive ($0.6 \pm 0.4 \text{ days}^{-1}$) between 12 and 14 m depth, and

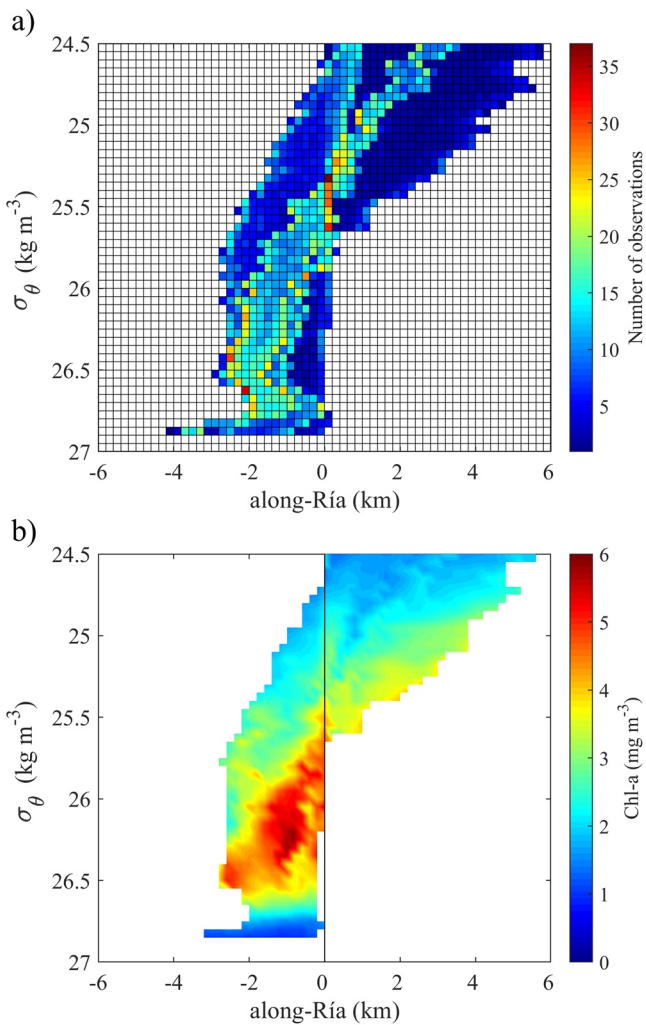


Figure 7. (a) Number of chlorophyll-a observations located at each $0.2 \text{ (km)} \times 0.01 \text{ (kg m}^{-3}\text{)} \text{ bin}$. (b) Reconstruction of the shape of the chlorophyll-a patch at the beginning of the cruise in the along-Ría axis by averaging chlorophyll-a values at each $0.2 \text{ (km)} \times 0.01 \text{ (kg m}^{-3}\text{)} \text{ bin}$. Solid vertical line indicates the position of the sampling station.

grangian transformation is capable of generating a spatially resolved view of chlorophyll-a fluorescence Eulerian observations, which improve the interpretation of local temporal variations.

As far as we know only a single study has previously applied this approach to oceanic chlorophyll-a fluorescence data: de Verneil and Franks (2015) used this technique to re-map Eulerian sampling locations and generate a corrected chlorophyll-a fluorescence map in the context of an ocean front in the California Current Ecosystem. Their pseudo-Lagrangian transformation re-mapped the ship track by back-advection and relocating sampling positions of observations acquired along streamlines, finally producing a transformed map of sampled data to appear as it would have if sampled instantaneously in space. Here, we have used the pseudo-Lagrangian method to re-map chlorophyll-a fluorescence profiles measured at a single fixed station over 27 h to reconstruct the spatial structure of a chlorophyll-a patch at single times.

Because current velocities were higher in the along-Ría axis, the reconstruction of the chlorophyll-a patch was only applied along this axis. Along-Ría residual currents were similar to those measured at the same station during June–July 2007, also in the transition from relaxation to upwelling conditions ($\pm 5 \text{ cm s}^{-1}$), and weaker than velocities reported during intense upwelling conditions ($> 10 \text{ cm s}^{-1}$) (Barton et al., 2015).

negative elsewhere. Values were fairly constant ($-0.3 \pm 0.1 \text{ d}^{-1}$) below 17 m, and slightly lower ($-0.5 \pm 0.2 \text{ days}^{-1}$) above 10 m. However, when averaged over the vertical extent of the patch maximum (chlorophyll-a $> 3 \text{ mg m}^{-3}$), biomass-normalized net rate of chlorophyll-a change was neutral ($-0.001 \pm 0.449 \text{ days}^{-1}$). Cell sinking estimated for diatoms of representative size and net biological production were the main and counterbalancing contributors to the observed chlorophyll-a net rate of change (Figure 11d). After removing the physical fluxes, net biological production was found to be positive ($0.28\text{--}1.32 \text{ days}^{-1}$) in the upper 15 m (i.e., above the chlorophyll-a maximum), with a local maximum at 12 m, and negative below, with minimum values (-1.28 days^{-1}) at 20 m depth. Taking into account the uncertainties in the determination of the different terms, mean net biological production in the upper 15 m was $0.53 \pm 0.25 \text{ days}^{-1}$ ($\pm \text{SD}$, standard deviation), while in deeper layers it was $-0.80 \pm 0.21 \text{ days}^{-1}$.

4. Discussion

4.1. Pseudo-Lagrangian Reconstruction of a Chlorophyll-a Patch

Here we present a proof-of-concept of a pseudo-Lagrangian approach applied to a time series of vertical profiles of chlorophyll-a fluorescence carried out at a single fixed station (Eulerian). The fact that the currents were dominated by the M2 tide and oscillated back and forth the sampling station allowed us to reconstruct the physical shape of a chlorophyll-a fluorescence patch that was advected several times past our sampling station. The approach begins by assuming that along-isopycnal flows were locally horizontally uniform, allowing us to reconstruct the spatial structure of the patch at any arbitrary time. Vertical shears in the horizontal velocities gave different patch shapes at different times. The reconstructed chlorophyll-a patch was tilted across isopycnals, consistent with the patch being sheared by low-frequency, vertically sheared upwelling currents over the course of the sampling campaign. The patch was thin and located on denser isopycnals toward the outer part of the Ría and thicker and associated with lighter isopycnals toward the inner part. This chlorophyll-a patch moved back and forth past the sampling station, modulated by the tidal and residual currents that controlled its shape and position during the sampling period. The residual deep inflow and the outflow at sub-surface depths intensified at the end of the sampling, changing the shape of the patch and causing it to become more vertical. Thus, the pseudo-Lagrangian transformation is capable of generating a spatially resolved view of chlorophyll-a fluorescence Eulerian observations, which improve the interpretation of local temporal variations.

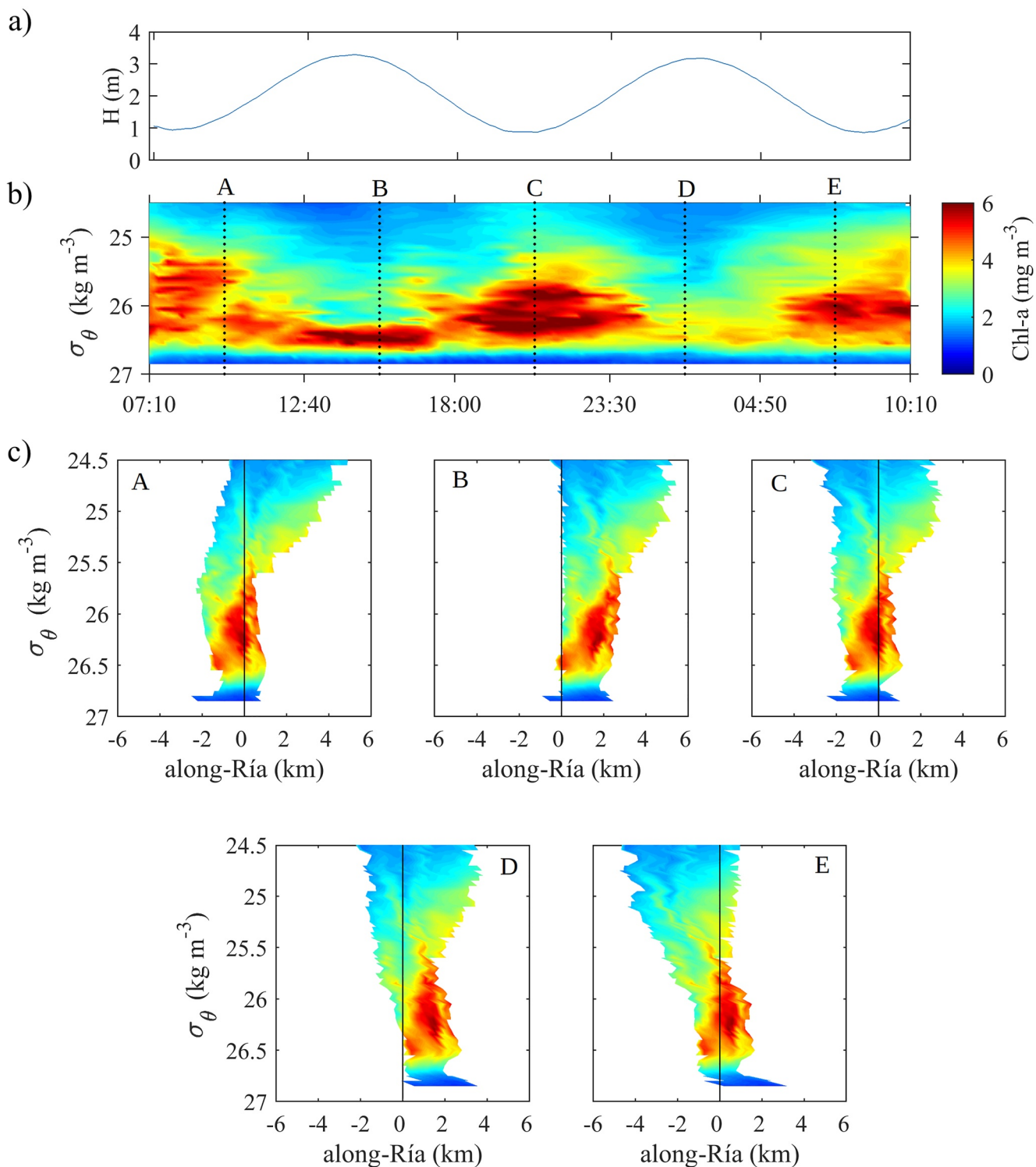


Figure 8. (a) Tidal height. (b) Eulerian distribution of chlorophyll-a in a vertical axis of potential density. (c) Sequential steps of the shape of the chlorophyll-a patch at (a) August 5, 2013 09:50, (b) August 5, 2013 15:20, (c) August 5, 2013 20:50, (d) August 6, 2013 02:10, and (e) August 6, 2013 07:30. Solid vertical line indicates the position of the sampling station.

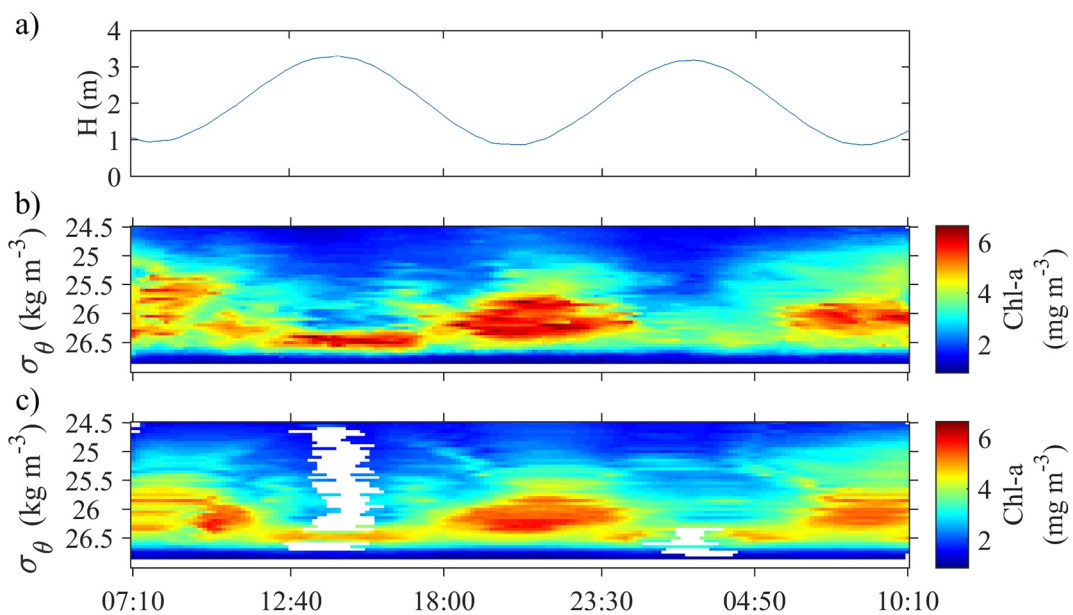


Figure 9. (a) Tidal height. (b) Original observed chlorophyll-a time series as a function of potential density. (c) Reconstructed chlorophyll-a time series from the pseudo-Lagrangian method. Horizontal scale corresponds to Coordinated Universal Time (UTC); local time was UTC+2.

Our sampling took place during a period of relaxation, when residual currents were not very important and the tidal currents dominated, moving the patch back and forth past our sampling site. Although residual currents were weak, the background shear induced by the bi-directional upwelling circulation caused the straining of the patch and its deformation over the course of the experiment. Furthermore, upwelling intensified toward the end of the sampling period, coinciding with an increase of ε and K_z values at intermediate depths, consistent with the background shear altering the shape of the chlorophyll-a patch by triggering turbulence and mixing. Shear-instability mixing has already been observed in the Ría de Vigo, caused by the interaction of wind-driven upwelling and tidal currents (Fernández-Castro et al., 2018). Vertical mixing could have contributed to the thickening of the patch over the sampling period. With a mean vertical diffusion around the chlorophyll-a maximum (8–20 m) of $K_z = 3.45 \pm 0.33 \times 10^{-5} \text{ m}^2 \text{ s}^{-1}$ ($\pm \text{SE}$, standard error), the patch would have increased its vertical extent by $\Delta h = \sqrt{2 K_z t} \approx 2.6 \text{ m}$ over 27 hr. This variation is smaller than the changes observed over a single tidal period, indicating that straining due to vertical shear and horizontal inhomogeneity of the patch were the main drivers of the changes in chlorophyll-a distribution found at tidal timescales in the Eulerian observation.

4.2. Estimation of Chlorophyll-a Net Rate of Change

One application of the pseudo-Lagrangian transformation is the estimation of the chlorophyll-a net rates of change in the sampled patch. This can be accomplished when the same water parcel is sampled at different times, allowing quantification of temporal changes in Chl-a concentration. This method computes the chlorophyll-a net rate of change following a water parcel, due to all biological and physical processes combined. This is a particularly useful calculation, as significant effort is typically required to characterize the processes that control chlorophyll-a concentration in the ocean, and most of them are not amenable to direct observation.

Using the same methodology as in this study, de Verneil and Franks (2015) reported 156 independent estimates with a mean net growth rate of -0.167 days^{-1} . They applied the pseudo-Lagrangian transformation to data measured from an underway survey and not at a fixed single point. Our chlorophyll-a net rates of change estimated using the pseudo-Lagrangian approach were close to zero when averaged over the patch maximum ($-0.001 \pm 0.449 \text{ days}^{-1}$ for chlorophyll-a $> 3 \text{ mg m}^{-3}$). However, these rates showed vertical variability, with some positive values just above the chlorophyll-a maximum and negative values for shallower

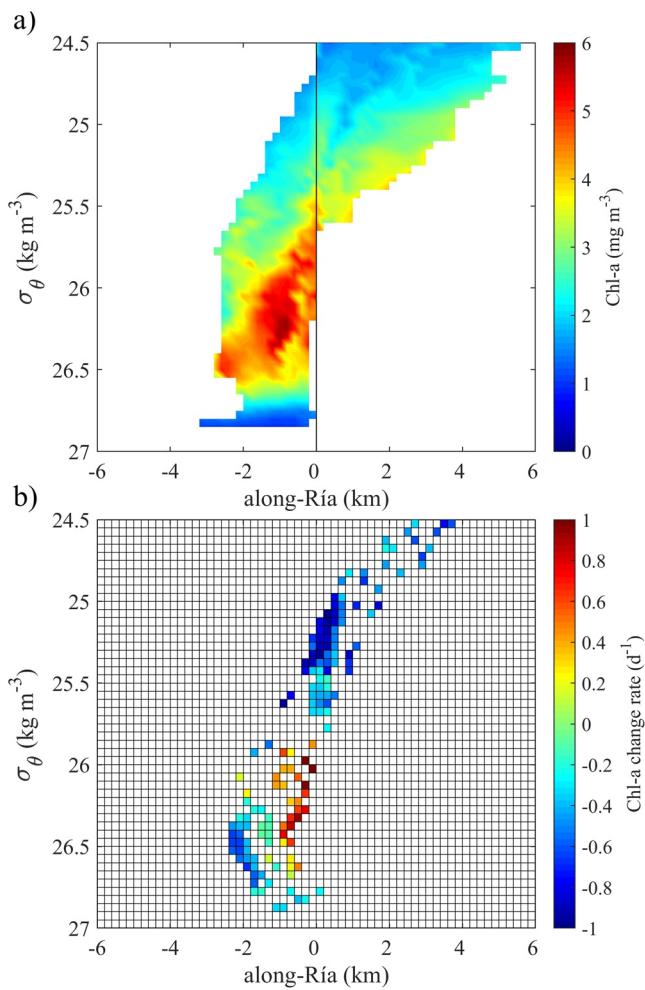


Figure 10. (a) Reconstruction of the shape of the chlorophyll-a patch at the beginning of the cruise in the along-Ría axis. (b) Net rates of change of chlorophyll-a in the $0.2\text{ (km)} \times 0.01\text{ (kg m}^{-3}\text{)}$ bins sampled at least twice within a time interval longer than 6 h.

and deeper waters. A simple 1-D evaluation of diffusion and sinking terms showed that the rates of chlorophyll-a change were dominated by biological and sinking processes at all depths.

The rates of phytoplankton growth and loss from grazing are commonly measured with the dilution method (Landry & Hassett, 1982). Teixeira and Figueiras (2009) measured surface chlorophyll-a growth and grazing rates by dilution experiments in the Ría de Vigo once every 2 months over a year. They reported phytoplankton net growth rates (growth minus mortality) ranging from -0.07 days^{-1} (July) to 1.06 days^{-1} (September). The averaged value for the upwelling season (April–September) was $0.2 \pm 0.7\text{ days}^{-1}$, reflecting the high variability of these rates in the Ría de Vigo. This value was comparable to our estimate of averaged net biological production rate (J_B) in the upper 15 m ($0.53 \pm 0.25\text{ days}^{-1}$).

5. Outlook

The feasibility of a pseudo-Lagrangian approach has been demonstrated by transforming chlorophyll-a fluorescence data from an Eulerian to a pseudo-Lagrangian frame of reference, generating a spatially resolved view of temporal observations recorded at a single fixed station. This approximation was possible because of the oscillatory tidal currents moved water parcels back and forth past the sampling station multiple times, thus yielding multiple samples of the same water at different times. The method could be successfully applied to the data from our survey because it took place during upwelling relaxation in which the residual currents were not very important and the tidal currents dominated, until the upwelling intensified toward the end of the sampling period. The pseudo-Lagrangian method permitted us to estimate chlorophyll-a net rates of change in the observed patch, including the net contributions of all biological and physical processes. By estimating the contributions of diffusion and sinking, we obtained estimates of the net biological production that were comparable with in vitro measurements of the balance between phytoplankton growth and mortality obtained from dilution experiments. However, care must be taken when comparing these in vitro measurements with our pseudo-Lagrangian estimates, since the latter did not include measurements of the phytoplankton community structure in

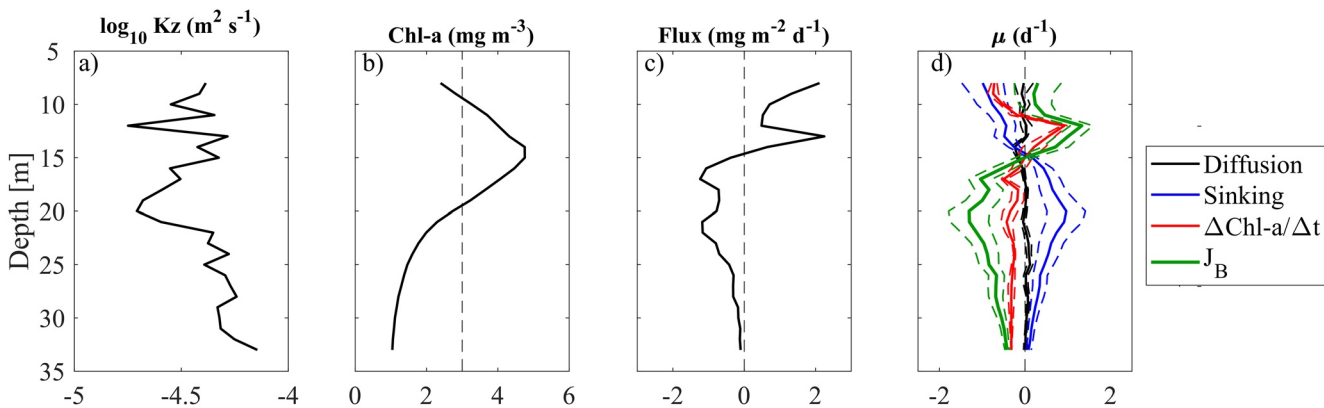


Figure 11. Depth profiles of (a) the logarithm of mean vertical diffusivity coefficient (K_z), (b) mean chlorophyll-a concentration, (c) chlorophyll-a diffusive flux, and (d) diffusion rate (black line), sinking rate (blue line), total chlorophyll-a change rate (red line), biological net production rate (J_B ; green line). Dashed lines in (d) represent standard errors propagated with a Monte Carlo approach.

the patch. Thus, future experiments of this type should include measurements of phytoplankton community composition. This will allow to determine the need to include a swimming term and also to refine the calculation of cell sinking velocity. In this regard, submersible camera systems represent promising options for observing marine organisms without perturbing or physically contacting the target objects (Giering et al., 2020). Moreover, *in vitro* experiments to estimate growth and mortality rates should be carried out simultaneously. Finally, sampling strategies combining high-resolution temporal but also spatial data (Broullón et al., 2021) will be needed in order to describe the horizontal uniformity in the flow and chlorophyll-a fields. This would allow to determine the validity of the assumptions required for the 1D (along-Ría axis) approach carried in this study, and even evaluate the possibility for a 2D approach (along and across Ría axes). Despite their limitations, these chlorophyll-a fluorescence net rate of change estimates derived from the pseudo-Lagrangian transformation are a useful complement to data obtained from traditional analyses for the quantification of ecological processes and biogeochemical budgets.

Data Availability Statement

The data analyzed in this study can be obtained from data server at the CSIC (Consejo Superior de Investigaciones Científicas, <https://nube.iim.csic.es/index.php/s/f7YcRZ4Z7LQikKJ>).

Acknowledgments

We are grateful to all the technicians, researchers and crew on board the R/V *Mytilus* for their help during field work. We also thank P. Chouciño, R. Graña and F. de la Granda for microstructure turbulence data collection and processing. This research was funded by projects: STRAMIX (CTM2012-35155) to Miguel Gilcoto and REMEDIOS (CTM2016-75451-C2-1-R) to B. Mourino-Carballedo from the Spanish Ministry of Economy and Competitiveness. M. Villamaña acknowledges the receipt of a FPU fellowship (FPU014/05,385) from the Spanish Ministry of Education, Culture and Sports. B. Fernández Castro was supported by the European Union's Horizon 2020 research and innovation program under the Marie Skłodowska-Curie Grant Agreement No. 834330 (SO-CUP). Funding for open access charge: Universidad de Vigo/CISUG.

References

- Álvarez-Salgado, X. A., Gago, J., Miguez, B. M., Gilcoto, M., & Pérez, F. F. (2000). Surface waters of the NW Iberian margin: Upwelling on the shelf versus outwelling of upwelled waters from the Rías Baixas. *Estuarine, Coastal and Shelf Science*, 51(6), 821–837. <https://doi.org/10.1006/ecss.2000.0714>
- Barton, E. D., Largier, J. L., Torres, R., Sheridan, M., Trasviña, A., Souza, A., et al. (2015). Coastal upwelling and downwelling forcing of circulation in a semi-enclosed bay: Ria de Vigo. *Progress in Oceanography*, 134, 1–189. <https://doi.org/10.1016/j.pocean.2015.01.014>
- Barton, E. D., Torres, R., Figueiras, F. G., Gilcoto, M., & Largier, J. L. (2016). Surface water subduction during a downwelling event in a semienclosed bay. *Journal of Geophysical Research*, 121(7088–7107), 3372–3380. <https://doi.org/10.1002/2015JC011421>
- Blanton, J. O., Tenore, K. R., Castillejo, F., Atkinson, L. P., Schweng, F. B., & Lavin, A. (1987). Relationship of upwelling to mussel production in the Rias on the western coast of Spain. *Journal of Marine Research*, 45(2), 497–511. <https://doi.org/10.1357/002224087788401115>
- Bowman, K. P., Lin, J. C., Stohl, A., Draxler, R., Konopka, P., Andrews, A., & Brunner, D. (2013). Input data requirements for Lagrangian trajectory models. *Bulletin of the American Meteorological Society*, 94(7), 1051–1058. <https://doi.org/10.1175/BAMS-D-12-00076.1>
- Broullón, E., Franks, P. J. S., Fernández Castro, B., Gilcoto, M., & Mourino-Carballedo, B. (2021). Rapid fluctuations of the subsurface chlorophyll maximum in response to wind forcing in a Long, Narrow Bay. *Earth and Space Science Open Archive*, 12. <https://doi.org/10.1002/essoar.10507856.1>
- Cermeno, P., Marañón, E., Pérez, V., Serret, P., Fernández, E., Castro, C. C., et al. (2006). Phytoplankton size structure and primary production in a highly dynamic coastal ecosystem (Ria de Vigo, NW-Spain): Seasonal and short-time scale variability. *Estuarine, Coastal and Shelf Science*, 67(1–2), 251–266. <https://doi.org/10.1016/j.ecss.2005.11.027>
- de Verneil, A., & Franks, P. J. S. (2015). A pseudo-Lagrangian method for remapping ocean biogeochemical tracer data: Calculation of net Chl-a growth rates. *Journal of Geophysical Research: Oceans*, 120(2), 7237–7252. <https://doi.org/10.1002/2015JC010969>
- Doglioli, A. M., Veneziani, M., Blanke, B., Speich, S., & Griffa, A. (2006). A Lagrangian analysis of the Indian-Atlantic interocean exchange in a regional model. *Geophysical Research Letters*, 33(14), 1–5. <https://doi.org/10.1029/2006GL026498>
- d'Ovidio, F., De Monte, S., Alvain, S., Dandonneau, Y., & Levy, M. (2010). Fluid dynamical niches of phytoplankton types. *Proceedings of the National Academy of Sciences*, 107(43), 18366–18370. <https://doi.org/10.1073/pnas.1004620107>
- d'Ovidio, F., Fernández, V., Hernández-García, E., & López, C. (2004). Mixing structures in the Mediterranean Sea from finite-size Lyapunov exponents. *Geophysical Research Letters*, 31(17), 1–n. <https://doi.org/10.1029/2004GL020328>
- Dragani, R., Redaelli, G., Visconti, G., Mariotti, a., Rudakov, V., Mackenzie, A. R., & Stefanutti, L. (2002). High resolution stratospheric tracer fields reconstructed with Lagrangian techniques: A comparative analysis of predictive skill. *Journal of the Atmospheric Sciences*, 59, 1943–1958. [https://doi.org/10.1175/1520-0469\(2002\)059<1943:HRSTFR>2.0.CO;2](https://doi.org/10.1175/1520-0469(2002)059<1943:HRSTFR>2.0.CO;2)
- Fernández-Castro, B., Gilcoto, M., Naveira-Garabato, A. C., Villamaña, M., Graña, R., & Mourino-Carballedo, B. (2018). Modulation of the semiidiurnal cycle of turbulent dissipation by wind-driven upwelling in a coastal embayment. *Journal of Geophysical Research: Oceans*, 123(6), 4034–4054. <https://doi.org/10.1002/2017JC013582>
- Fernández-Castro, B., Mourino-Carballedo, B., Benítez-Barrios, V. M., Chouciño, P., Fraile-Nuez, E., Graña, R., et al. (2014). Microstructure turbulence and diffusivity parameterization in the tropical and subtropical Atlantic, Pacific and Indian Oceans during the Malaspina 2010 expedition. *Deep-Sea Research Part I: Oceanographic Research Papers*, 94, 15–30. <https://doi.org/10.1016/j.dsr.2014.08.006>
- Figueiras, F. G., Labarta, U., & Fernández Reiriz, M. J. (2002). Coastal upwelling, primary production and mussel growth in the Rías Baixas of Galicia. *Hydrobiologia*, 484, 121–131. <https://doi.org/10.1023/A:1021309222459>
- Figueiras, F. G., & Niell, F. X. (1987). Composición del fitoplancton de la ría de Pontevedra. *Investigación Pesquera*, 51, 371–409.
- Figueiras, F. G., & Pazos, Y. (1991). Microplankton assemblages in three Rias Baixas (Vigo, Arosa and Muros, Spain) with a subsurface chlorophyll maximum: Their relationships to hydrography. *Marine Ecology Progress Series*, 76, 219–233. <https://doi.org/10.3354/meps076219>
- Giering, S. L. C., Cavan, E. L., Basedow, S. L., Briggs, N., Burd, A. B., Darroch, L. J., et al. (2020). Sinking organic particles in the ocean—flux estimates from *in situ* optical devices. *Frontiers in Marine Science*, 6(February). <https://doi.org/10.3389/fmars.2019.00834>
- Gilcoto, M., Álvarez-Salgado, X. A., & Perez, F. F. (2001). Computing optimum estuarine residual fluxes with a multiparameter inverse method (OERFM): Application to the Ria de Vigo (NW Spain). *Journal of Geophysical Research*, 106(31), 303318–303334. <https://doi.org/10.1029/2000jc000665>

- Gilcoto, M., Largier, J. L., Barton, E. D., Piedracoba, S., Torres, R., Graña, R., et al. (2017). Rapid response to coastal upwelling in a semi-enclosed bay. *Geophysical Research Letters*, 44(5), 2388–2397. <https://doi.org/10.1002/2016GL072416>
- Godin, G. (1972). *The analysis of tides*. University of Toronto Press.
- Gregg, M. C., D'Asaro, E. A., Riley, J. J., & Kunze, E. (2018). Mixing efficiency in the ocean. *Annual Review of Marine Science*, 10, 443–473. <https://doi.org/10.1146/annurev-marine-121916-063643>
- Landry, M. R., & Hassett, R. P. (1982). Estimating the grazing impact of marine micro-zooplankton. *Marine Biology*, 67(3), 283–288. <https://doi.org/10.1007/BF00397668>
- Miklasz, K. A., & Denny, M. W. (2010). Diatom sinking speeds: Improved predictions and insight from a modified Stoke's law. *Limnology & Oceanography*, 55(6), 2513–2525. <https://doi.org/10.4319/lo.2010.55.6.2513>
- Mouriño-Carballedo, B., Otero Ferrer, J. L., Fernández-Castro, B., Marañón, E., Blazquez Maseda, M., Aguiar-González, B., et al. (2021). Magnitude of nitrate turbulent diffusion in contrasting marine environments. *Scientific Reports*, 11. <https://doi.org/10.1038/s41598-021-97731-4>
- Nilsson, E. D., & Leck, C. (2002). A pseudo-Lagrangian study of the sulfur budget in the remote Arctic marine boundary layer. *Tellus Series B Chemical and Physical Meteorology*, 54(3), 213–230. <https://doi.org/10.1034/j.1600-0889.2002.01247.x>
- Osborn, T. R. (1980). Estimates of the local rate of vertical diffusion from dissipation measurements. *Journal of Physical Oceanography*, 10(1), 83–89. [https://doi.org/10.1175/1520-0485\(1980\)010<0083:eotlro>2.0.co;2](https://doi.org/10.1175/1520-0485(1980)010<0083:eotlro>2.0.co;2)
- Piedracoba, S., Álvarez-Salgado, X. A., Rosón, G., & Herrera, J. L. (2005). Short-timescale thermohaline variability and residual circulation in the central segment of the coastal upwelling system of the Ría de Vigo (northwest Spain) during four contrasting periods. *Journal of Geophysical Research*, 110(C3), C03018. <https://doi.org/10.1029/2004JC002556>
- Pitcher, G. C., Figueiras, F. G., Hickey, B. M., & Moita, M. T. (2010). The physical oceanography of upwelling systems and the development of harmful algal blooms. *Progress in Oceanography*, 85(1–2), 5–32. <https://doi.org/10.1016/j.pocean.2010.02.002>
- Prandke, H., & Stips, A. (1998). Test measurements with an operational microstructure-turbulence profiler: Detection limit of dissipation rates. *Aquatic Sciences*, 60(3), 191–209. <https://doi.org/10.1007/s000270050036>
- Ríos, A. F., Pérez, F. F., & Fraga, F. (1992). Water masses in the upper and middle North Atlantic east of the Azores. *Deep-Sea Research Part A*, 39(3–4), 645–658. [https://doi.org/10.1016/0198-0149\(92\)90093-9](https://doi.org/10.1016/0198-0149(92)90093-9)
- Smyth, W. D. (2020). Marginal instability and the efficiency of ocean mixing. *Journal of Physical Oceanography*, 50(8), 2141–2150. <https://doi.org/10.1175/JPO-D-20-0083.1>
- Teixeira, I. G., & Figueiras, F. G. (2009). Feeding behaviour and non-linear responses in dilution experiments in a coastal upwelling system. *Aquatic Microbial Ecology*, 55(1), 53–63. <https://doi.org/10.3354/ame01281>
- Villamaña, M., Mouriño-Carballedo, B., Marañón, E., Cermeño, P., Chouciño, P., da Silva, J. C. B., et al. (2017). Role of internal waves on mixing, nutrient supply and phytoplankton community structure during spring and neap tides in the upwelling ecosystem of Ría de Vigo (NW Iberian Peninsula). *Limnology & Oceanography*, 62(3), 1014–1030. <https://doi.org/10.1002/lo.10482>
- Wong, K.-C., & Moses-Hall, J. E. (1998). The tidal and subtidal variations in the transverse salinity and current distributions across a coastal plain estuary. *Journal of Marine Research*, 56(2), 489–517. <https://doi.org/10.1357/002224098321822393>